

Bridging Human Evaluation to Infrared and Visible Image Fusion

Jinyuan Liu¹, Xingyuan Li², Qingyun Mei³, Haoyuan Xu³,
Zhiying Jiang⁴, Long Ma³, Risheng Liu³, Xin Fan^{3*}

¹ School of Mechanical Engineering, Dalian University of Technology

² College of Computer Science and Technology, Zhejiang University

³ School of Software Technology & DUT-RU International School of ISE, Dalian University of Technology

⁴ College of Information Science and Technology, Dalian Maritime University

atlantis918@hotmail.com xin.fan@dlut.edu.cn

Abstract

Infrared and visible image fusion (IVIF) integrates complementary modalities to enhance scene perception. Current methods predominantly focus on optimizing handcrafted losses and objective metrics, often resulting in fusion outcomes that do not align with human visual preferences. This challenge is further exacerbated by the ill-posed nature of IVIF, which severely limits its effectiveness in human perceptual environments such as security surveillance and driver assistance systems. To address these limitations, we propose a feedback reinforcement framework that bridges human evaluation to infrared and visible image fusion. To address the lack of human-centric evaluation metrics and data, we introduce the first large-scale human feedback dataset for IVIF, containing multidimensional subjective scores and artifact annotations, and enriched by a fine-tuned large language model with expert review. Based on this dataset, we design a domain-specific reward function and train a reward model to quantify perceptual quality. Guided by this reward, we fine-tune the fusion network through Group Relative Policy Optimization, achieving state-of-the-art performance that better aligns fused images with human aesthetics. Code is available at <https://github.com/ALKA-Wind/EVAFusion>.

1. Introduction

Infrared and visible image fusion (IVIF) stands as a pivotal technique in computational imaging, aiming to synthesize a single image that comprehensively preserves the thermal radiation information from infrared images and the rich textual details from visible images [42, 60, 66, 72]. This complementary fusion paradigm is crucial for a wide spectrum of high-stakes applications, including autonomous driv-

ing [27], security surveillance [61], medical imaging [68], remote sensing [62], and military reconnaissance [9].

Despite significant advancements, the fundamental goal of IVIF is to generate a fused image that is preferable for human observation and analysis, remaining inadequately addressed. The task is inherently ill-posed due to the absence of a unique ground-truth fusion result [57]. Consequently, the field has long been dominated by the pursuit of optimizing handcrafted objective functions and numerical metrics, such as entropy, structural similarity, and gradient-based measures [26, 28, 56]. While these approaches have driven progress, they suffer from a critical limitation: **the discrepancy between these mathematical proxies and genuine human perceptual preferences.**

Recent deep learning-based methods, particularly those employing generative models [22, 32, 36, 41, 43] and attention mechanisms [15, 23], have demonstrated powerful capabilities in feature extraction and fusion. However, they largely inherit the same evaluation paradigm, training networks with pixel-level or feature-level losses that are ultimately divorced from human judgment. This creates a significant gap: current fusion models are not explicitly optimized to produce outputs that align with human aesthetic and perceptual consistency. The root causes of this gap are twofold: (1) the lack of a large-scale, high-quality dataset containing human feedback on IVIF results, (2) the absence of a reliable and automated reward mechanism to quantify perceptual quality and guide the model’s learning process.

To bridge this critical gap, we introduce a novel Feedback Reinforcement Framework that directly integrates subjective human evaluation into the IVIF pipeline. Our work is built upon the core insight that human preference should be the ultimate supervisor for this ill-posed task. The key challenge lies in efficiently and scalably incorporating this expensive, subjective feedback into the optimization loop.

Specifically, we first constructed a comprehensive human feedback dataset comprising subjective assessments

*Corresponding author.

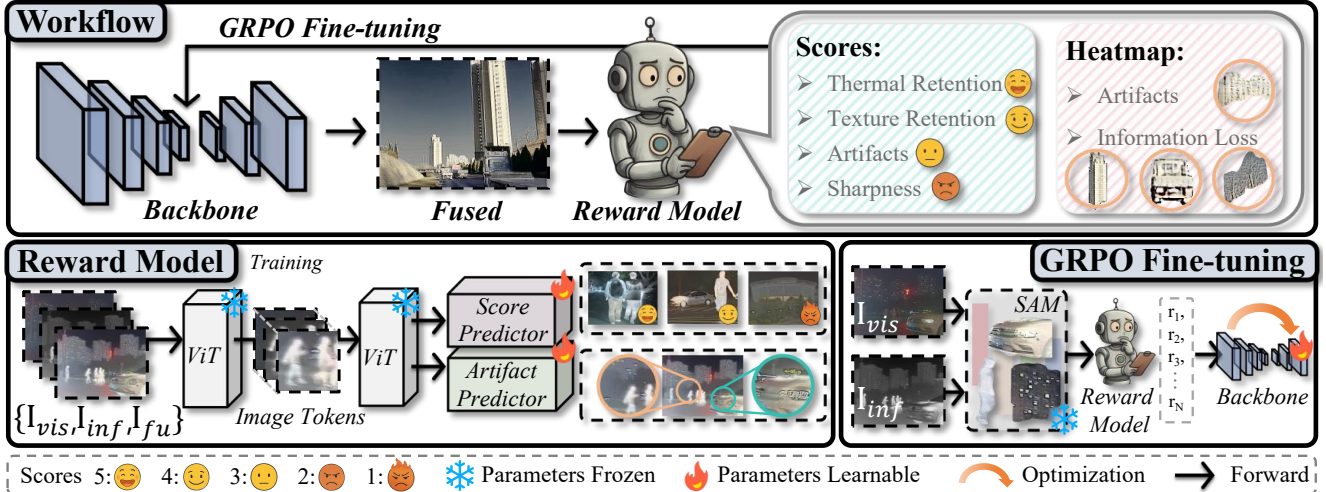


Figure 1. **Illustration of our pipeline.** The fine-tuning module is based on RLHF, integrating the ViT-based fusion-oriented reward model trained with the Human Feedback Dataset. A segmentation-assisted mechanism, based on GRPO, is introduced for fine-tuning, aiming to improve the quality of the fused images.

and artifact annotations for fused images. This dataset includes 850 image pairs drawn from eight diverse datasets, fused by eleven representative models to generate 9,350 images. To efficiently and accurately annotate this large dataset, we employed GPT-4o based on expert-labeled samples. Then, we leveraged the model to assist in scoring and annotation, with expert review to ensure quality. Using this dataset, we designed a specialized reward function and trained a reward model to capture human perceptual preferences quantitatively. Finally, guided by this reward model, we fine-tuned existing fusion networks using Group Relative Policy Optimization (GRPO), achieving state-of-the-art performance that better reflects human aesthetic judgments. Our main contributions are summarized as follows:

- We propose a feedback reinforcement IVIF framework that explicitly integrates subjective human preferences into the fusion process, effectively bridging the gap between objective image quality metrics and human perceptual consistency.
- To address the lack of human-centric evaluation data, we construct the first large-scale, high-quality human feedback dataset in the IVIF domain, featuring multidimensional subjective scores and detailed artifact annotations.
- We develop a reward function and a tailored reinforcement learning strategy for IVIF, enabling fusion models to better capture human visual preferences and achieve state-of-the-art performance.

2. Related works

2.1. Infrared and Visible Image fusion

As an important image enhancement technique, infrared and visible image fusion has continued to attract increasing

attention in recent years [2, 5, 16, 17, 21, 48, 50]. With the rapid development of deep learning, deep learning-based image fusion methods have gradually become a research hotspot. Convolutional Neural Networks (CNNs) have become a common method for image fusion [3, 19, 34], such as CoCoNet [29], which optimizes the fusion process through data-sensitive weights. Generative Adversarial Networks (GANs) have also demonstrated advantages in image fusion tasks [18, 32, 55], like GANMcC [33], which introduces multi-classification constraints. The Transformer model, known for handling long-range dependencies, has been applied to image fusion [20, 35, 40], such as PromptFusion [28], which combines Vision-Language models to enhance target recognition. Additionally, diffusion models like DDFM [47, 54, 69] have improved the realism of fused images, and TIMFusion [31] introduces semantic segmentation to improve fusion quality under unsupervised learning. However, these methods predominantly optimize handcrafted losses and objective metrics, lacking alignment with human perceptual preferences.

2.2. Human Feedback Reinforcement Learning

Reinforcement Learning from Human Feedback (RLHF) was first introduced by Christiano et al. [6], demonstrating performance that surpassed conventional deep learning paradigms. Its core lies in using human preferences as optimization objectives, training reward models to align with human value judgments, thereby guiding the learning process of policy models. RLHF was initially applied in natural language processing (NLP). InstructGPT [39], which significantly improved GPT-3’s instruction-following capability. Subsequently, models like Qwen [1], DeepSeeker-V3 [25], and LLaMA-2 [52] have also validated the effective-

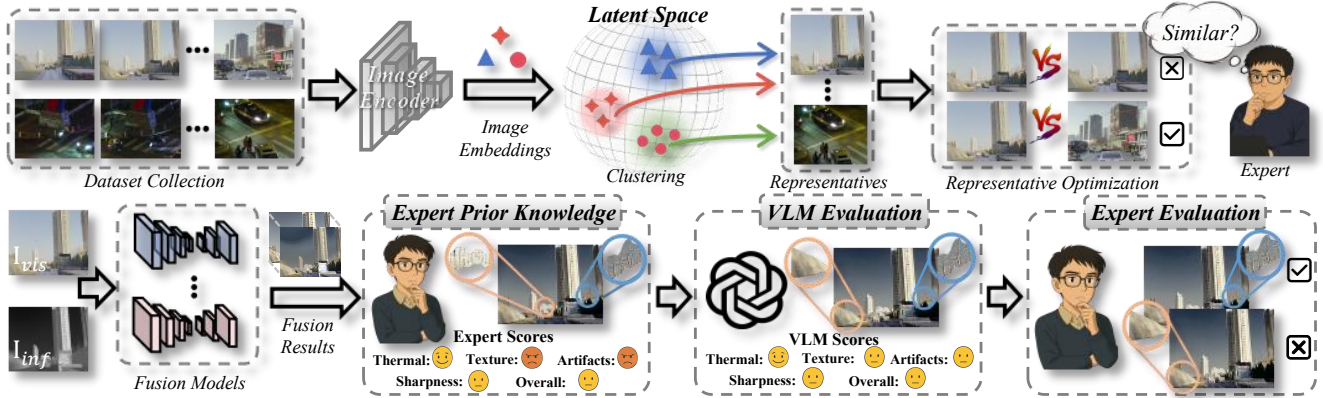


Figure 2. **Workflow of the dataset collection.** The dataset is processed and clustered to optimize representative images, followed by expert screening. Use fusion models to fuse I_{vis} and I_{inf} images, with experts scoring and annotating a subset as prior knowledge for aligning the GPT model. After GPT annotates all images, experts review the results, resulting in the human feedback IVIF dataset.

tiveness of RLHF. Building on this, RLHF has been extended to the field of computer vision, improving tasks such as text-to-image generation [7, 24] and text-to-video refinement [63]. Methods like DPOK [8] and ImageReward [59] have enhanced the quality of generated results by providing reliable reward signals through human feedback. The success of RLHF in both NLP and CV demonstrates its effectiveness in optimizing model performance.

3. Method

This section details our framework, including the creation of the human feedback dataset, the construction of the reward model, and the fine-tuning process of the fusion network, as illustrated in Fig. 1.

3.1. Human Preference-Aligned Dataset for IVIF

Dataset Collection. Fig. 2 shows the process of collecting human feedback data and constructing the dataset. To address the inconsistency between existing infrared-visible image fusion (IVIF) methods and human visual preferences in terms of visual quality, we constructed a human feedback IVIF dataset to support the modeling and evaluation of perceptual consistency. We first collected more than 30,000 pairs of infrared-visible images from the FMB [27], LLVIP [13], M³FD [26], MFNet [10], RoadScene [57], SMOD [4], TNO [51], and VIFB [65] datasets. These images cover a wide range of scenes and environmental conditions. Considering the potential presence of numerous duplicate scenes in the dataset, we used the CLIP model for data cleaning. This process resulted in 900 pairs of infrared-visible images. Further expert screening was conducted on the CLIP-cleaned data, ultimately yielding 850 pairs of high-quality images. We then conducted inference eleven SOTA methods: MURF [58], DDcGAN [56], MetaFusion [67], PromptF [28], CDDfuse [68], SegMif [27],

Text-IF [61], DDFM [69], U2Fusion [57], CoCoNet [29], and TarDAL [26]. This resulted in the generation of 9,350 fused images.

Large Models and Human Feedback Annotation. To obtain high-quality annotated fusion data that comprehensively reflects human visual preferences, we adopted a collaborative annotation process combining expert knowledge with large language models. Each fused image is assigned four fine-grained scores (1-5 scale), a total average score, and a heatmap. The fine-grained scores include: thermal retention, texture retention, artifacts level, and sharpness. Additionally, the heatmap highlights regions in the fused image where artifacts are particularly noticeable. We first invited four senior experts with over five years of IVIF research experience to perform refined scoring on 100 fused images and annotate artifact regions using center coordinates and radii. This resulted in a high-quality seed dataset of 100 images, covering the full spectrum of IVIF scenes with diverse environmental conditions and quality levels, maximizing the information density of each sample.

GPT-4o [12] was trained using RLHF on large-scale multimodal datasets, learning knowledge about visual perception and human preferences, allowing the model’s outputs to align with human perception. Therefore, we fine-tuned the GPT-4o model using the seed dataset to enable it to automatically assign refined scores and locate artifacts in fused images. The GPT-4o was then used to annotate all 9,350 fused images. To ensure the accuracy of these automated annotations, after GPT-4o completed the annotations, we invited five researchers with at least three years of IVIF experience to thoroughly review and refine the GPT-generated scores and heatmaps, including correcting deviations in scoring standards and supplementing missing artifact regions. The final human feedback IVIF dataset was used to train the fusion-oriented reward model. More details can be found in the supplementary material.

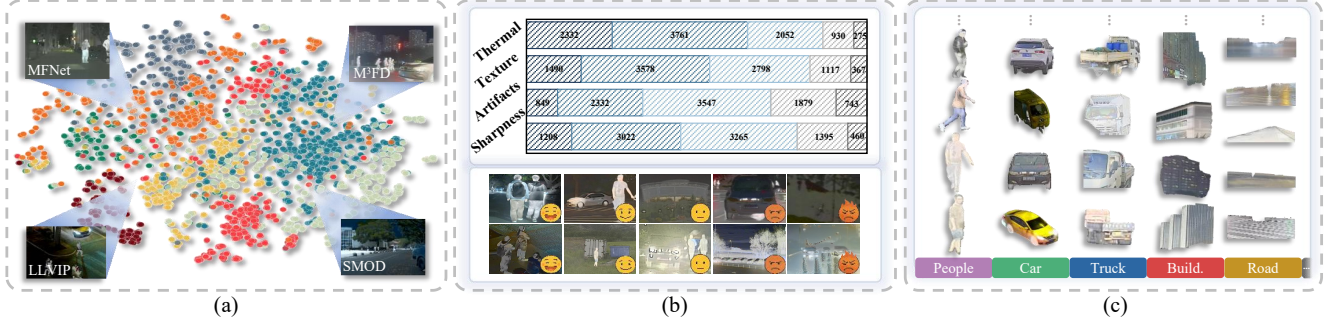


Figure 3. **Overview of our collected dataset.** (a) Data diversity: samples from multiple benchmark datasets; (b) Label diversity: each sample contains fine-grained scores across four quality dimensions and artifact heatmaps; (c) Scene diversity: covering key semantic categories including people, cars, buildings, roads, and more.

3.2. Fusion-Oriented Reward Model

To leverage human feedback for model optimization, we train a fusion-oriented reward model on the constructed dataset. The principal aim of the reward model is to provide a comprehensive representation of both the infrared and visible images, along with their corresponding fused image, to predict four fine-grained scores and identify the spatial distribution of artifact regions in the fused image.

To fully capture the global semantic information of the input image and achieve comprehensive modeling of both structural information and semantic features, we propose a Fusion-Oriented Reward Model based on the ViT-based vision-language model. During training, the parameters of the ViT module are kept frozen, and only the upper prediction head is optimized to enhance training stability and convergence efficiency. For each input sample pair, it includes an infrared image, a visible image, and a fused image, they are respectively fed into a weight-shared ViT encoder to obtain three sets of patch-level semantic representations: $F_i = \text{ViT}(x_i)[:, 1 :, :]$, for $x_i \in \{x_{\text{ir}}, x_{\text{vi}}, x_{\text{fused}}\}$. The above three sets of features are concatenated along the channel dimension as $[F_{\text{ir}} \parallel F_{\text{vi}} \parallel F_{\text{fused}}] \in \mathbb{R}^{N \times 3D}$, then compressed to the original dimensionality through a linear projection and fed into another ViT encoder with the same architecture for cross-modal feature fusion. The output of the fusion ViT is reshaped into a spatial feature map format, serving as the input to the subsequent prediction branch.

The feature map $\mathcal{F}_{\text{map}} \in \mathbb{R}^{D \times H' \times W'}$ is used as input and fed into two separate prediction branches. For the heatmap prediction branch, the fused feature map is first channel-compressed through a convolutional module, and then progressively upsampled with residual structures to restore spatial resolution. A single-channel heatmap is finally generated using a Sigmoid activation function, producing an artifact probability map with values in the range $[0,1]$, which highlights potential structural artifact regions in the image. For the score prediction branch, the feature map is sequentially compressed through convolutional layers, flat-

tened, and passed through a multilayer perceptron to regress each score value. The output is processed by a Sigmoid activation function, and the final result is a scalar representing the fine-grained score.

We train the model by jointly optimizing two loss terms. The Mean Squared Error (MSE) is used as the primary loss function. For each score dimension s_i and the heatmap label H , the corresponding loss terms are defined as:

$$\mathcal{L}_{\text{score}} = \sum_{i=1}^5 \text{MSE}(s_i, \hat{s}_i), \quad \mathcal{L}_{\text{heatmap}} = \text{MSE}(H, \hat{H}). \quad (1)$$

The final training objective is a weighted sum of the two:

$$\mathcal{L}_{\text{total}} = \lambda_1 \cdot \mathcal{L}_{\text{score}} + \lambda_2 \cdot \mathcal{L}_{\text{heatmap}}. \quad (2)$$

3.3. Policy Optimization for IVIF Model

As the foundation for our RLHF optimization, we adopt the Discriminative cross-Dimensional Evolutionary Learning (DCEvo) framework [30] as our baseline fusion network. DCEvo adopts an encoder-decoder structure, using Discriminative Enhancer and Cross-Dimensional Embedding modules for feature extraction and modeling. Although existing fusion networks have achieved satisfactory performance in integrating multimodal image information, their optimization objectives are primarily based on traditional image quality metrics and task accuracy, leaving room for improvement in subjective visual quality as well as the clarity and fidelity of critical target regions.

We propose an RLHF-driven policy optimization for the IVIF model to enhance the alignment between fusion results and human perceptual preferences and improve the model's ability to perceive critical semantic targets within images. Inspired by Group Relative Policy Optimization (GRPO) [46], we extract key semantic regions using the Segment Anything Model (SAM) [14] and compute region-level advantages. Specifically, for each pair of input visible and infrared images (v, i) , the fused image F generated by

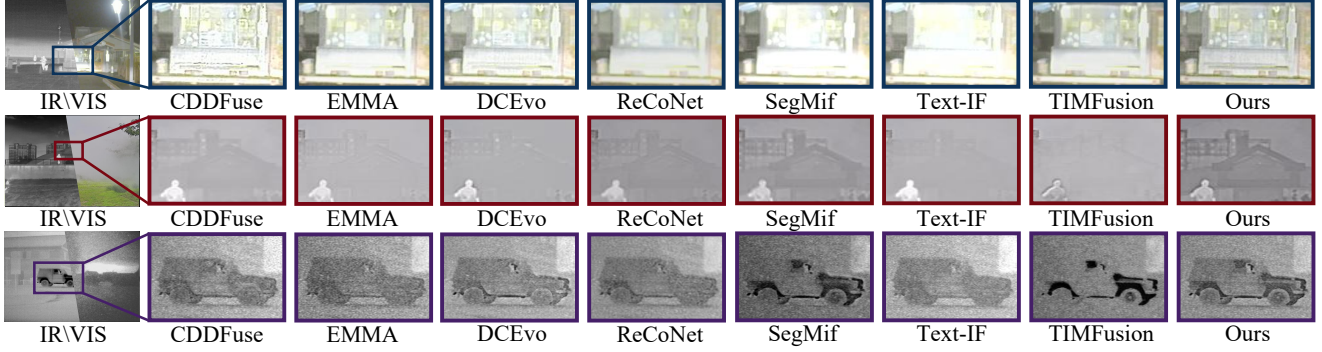


Figure 4. Qualitative comparison of our method with existing image fusion methods. From top to bottom: RoadScene, M³FD, TNO.

Table 1. Quantitative comparison of IVIF between our method and state-of-the-art methods on TNO, RoadScene, and M³FD datasets. Red and blue represent the best and second-best results.

Method	TNO				RoadScene				M ³ FD			
	CC \uparrow	PSNR \uparrow	Qabf \uparrow	SSIM \uparrow	CC \uparrow	PSNR \uparrow	Qabf \uparrow	SSIM \uparrow	CC \uparrow	PSNR \uparrow	Qabf \uparrow	SSIM \uparrow
CDDFuse [68]	0.47	63.49	0.49	<u>0.54</u>	0.52	59.84	0.43	0.45	0.62	63.14	0.61	0.51
DDFM [69]	0.44	63.40	0.17	0.03	0.41	59.40	0.15	0.03	0.65	<u>64.82</u>	0.48	<u>0.50</u>
EMMA [70]	0.45	63.10	0.42	0.49	0.50	59.71	0.42	0.44	0.58	63.35	0.57	0.46
LRRNet [15]	0.41	62.38	0.31	0.41	<u>0.53</u>	59.56	0.39	0.36	<u>0.63</u>	64.18	0.48	0.38
MRFS [64]	0.49	61.78	0.41	0.47	0.50	<u>61.46</u>	0.39	0.45	0.46	61.24	0.54	0.44
PromptF [28]	0.46	62.40	0.51	0.51	0.52	61.42	0.49	0.47	0.50	62.03	0.60	0.49
ReCoNet [11]	0.46	<u>64.81</u>	0.34	0.46	0.52	60.75	0.36	0.44	0.58	64.11	0.47	0.43
SegMif [27]	<u>0.50</u>	62.52	0.50	0.49	<u>0.53</u>	60.80	<u>0.51</u>	0.46	0.55	62.81	0.62	0.48
SHIP [71]	0.48	61.54	0.50	0.48	0.47	60.87	0.49	0.45	0.46	61.28	0.62	0.44
TarDAL [26]	0.47	63.94	0.43	0.53	0.48	60.59	0.40	0.44	0.57	63.85	0.41	0.46
Text-IF [61]	0.46	63.71	0.48	0.47	0.50	59.94	0.50	0.43	0.59	63.87	0.66	0.48
TIMFusion [31]	0.42	63.98	0.41	0.49	0.44	61.12	0.41	0.44	0.40	62.17	0.47	0.38
Dcevo[30]	0.48	63.83	0.55	0.53	0.49	59.66	0.50	<u>0.48</u>	0.55	62.87	<u>0.63</u>	0.47
Ours	0.51	65.43	<u>0.52</u>	0.56	0.56	61.84	0.53	0.50	0.65	65.09	<u>0.63</u>	0.49

the current fusion policy network π_θ is segmented by SAM into K segmented images $F\{f_1, \dots, f_K\}$, $f_k = F \odot \mathcal{M}_k$, where \mathcal{M}_k denotes the binary mask for region k . The segmented images, together with the fused image, are fed into the learned reward model (see Sec. 3.2) for evaluation, producing a set of multidimensional quality scores $F\{s_1, \dots, s_K\}$. Based on these scores, we compute the normalized relative advantage values within each group:

$$\mu = \frac{1}{K} \sum_{k=1}^K s_k, \quad \hat{A}_k = \frac{s_k - \mu}{\sigma + \epsilon}. \quad (3)$$

Subsequently, the fusion policy network π_θ is updated by maximizing the following objective (loss function):

$$\mathcal{J}(\theta) = \mathbb{E}_{(v,i)} [\mathcal{L}(\theta) - \beta \cdot D_{\text{KL}}[\pi_\theta | \pi_{\text{ref}}]], \quad (4)$$

$$\mathcal{L}(\theta) = \sum_{k=1}^K w_k \cdot \min \left(r_k \hat{A}_k, \text{clip}(r_k, 1 - \epsilon, 1 + \epsilon) \hat{A}_k \right), \quad (5)$$

where π_{ref} denotes the reference policy, which is a frozen copy of the current policy π_θ at the initial time step. $r_k =$

$1 + \alpha \cdot \frac{|F_\theta[\mathcal{M}_k] - F_{\theta_{\text{old}}}[\mathcal{M}_k]|}{|F_{\theta_{\text{old}}}[\mathcal{M}_k]|}$ measures the policy change for each region. D_{KL} denotes the KL divergence regularization term, which prevents the policy from deviating too far from the reference policy.

4. Experiments

4.1. Set up

Dataset. For the Fusion-Oriented Reward Model. As shown in Fig. 3, our human feedback dataset contains 9,350 samples from eight benchmark datasets, each consisting of a pair of infrared and visible images, a fused image, and corresponding fine-grained scores along with annotated artifact regions. The dataset is divided into 7,350 training samples, 1,000 validation samples, and 1,000 test samples. For RLHF-driven policy optimization and fusion experiments, we used the MSRS [49], RoadScene [57], M³FD [26], and TNO [51] datasets for training and evaluation.

Training Setup and Evaluation. To train the reward model, we adopt the ViT-Large-Patch16-384 model as the feature extractor, freezing its parameters, and train the score

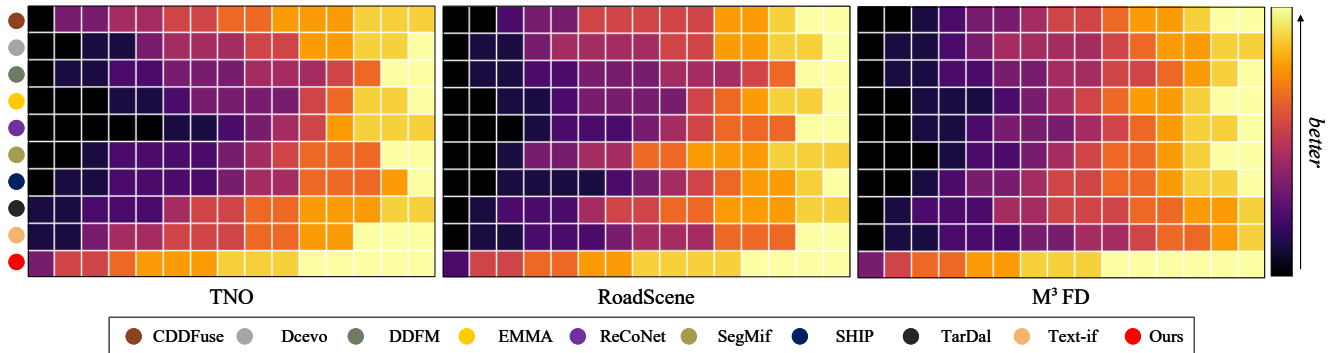


Figure 5. Preference ranking heatmaps on three datasets. Yellow represents the most preferred, and purple represents the least preferred.

Table 2. Quantitative comparison of IVIF between our method and other methods using no-reference image quality assessment metrics. **Red** and **blue** represent the best and second-best results.

Method	TNO		RoadScene		M ³ FD	
	NIQE↓	BRI*↓	NIQE↓	BRI*↓	NIQE↓	BRI*↓
CDDFuse [68]	7.43	37.62	3.26	24.74	4.37	32.88
DDFM [69]	7.54	34.28	3.32	27.19	5.05	38.78
EMMA [70]	6.33	26.08	4.93	22.20	5.45	35.16
LRRNet [15]	9.31	38.68	4.42	29.45	4.33	37.68
MRFS [64]	7.89	25.95	3.81	27.07	4.37	34.52
PromptF [28]	6.35	25.06	3.95	21.93	4.36	33.09
ReCoNet [11]	5.47	26.18	5.70	38.86	5.06	50.22
SegMif [27]	6.22	29.12	3.45	29.41	4.25	34.75
SHIP [71]	5.93	24.55	3.22	20.21	4.16	27.75
TarDAL [26]	5.76	35.76	4.19	32.04	4.20	37.37
Text-IF [61]	6.91	34.50	3.33	24.82	5.04	40.06
TIMFusion [31]	7.19	32.46	4.44	30.16	4.61	46.93
DCEvo [30]	6.25	33.97	3.13	22.31	4.48	35.93
Ours	5.37	22.58	3.06	18.79	4.03	29.80

predictor and heatmap generator for 30 epochs using the AdamW optimizer with cosine annealing learning rate from $2e-5$ to $1e-5$ and weight decay of $2e-3$. For RLHF-driven policy optimization, during fine-tuning, the KL divergence coefficient (β) is set to 0.1 and epsilon to 0.2. We use the Adam optimizer with a learning rate of $1e-4$, weight decay of 0.01, batch size of 2, and train for 20 epochs. The CosineAnnealingLR scheduler is employed with a decay factor of 0.5 and a minimum learning rate of $1e-6$.

We compare our method with 13 state-of-the-art methods using four reference-based metrics: Cross-Correlation (CC), Peak Signal-to-Noise Ratio (PSNR), Quality of Fused Image Based on Brightness and Focus (Qabf), and Structural Similarity Index (SSIM)[53], along with two no-reference metrics: NIQE[38] and BRISQUE [37]. All experiments in the paper were conducted on two A40 GPUs.

4.2. Infrared and visible image fusion results

To demonstrate the effectiveness of our method, we conduct both qualitative and quantitative comparisons against 13 ex-

isting state-of-the-art methods on three benchmark datasets.

The qualitative evaluation results shown in Fig. 4 demonstrate that our method effectively preserves and enhances important features from the infrared images, such as the structure of cars and buildings, especially in low-light and foggy scenes. Additionally, guided by human feedback, our method retains more texture details, making the fused images more aligned with human visual perception. The quantitative analysis presented in Tab. 1 and Tab. 2 shows that our method performs excellently in terms of PSNR, CC, Qabf, and SSIM, particularly achieving the highest CC and PSNR values across all three test sets. For the no-reference metrics NIQE and BRISQUE, our method also performs the best across the three test datasets, ranking first or second. These results fully demonstrate the superior fusion performance of our method.

4.3. Human Preference Analysis of Fusion Results

To further validate the effectiveness of our method in terms of human subjective preferences, we designed a subjective evaluation experiment to analyze the fusion quality of different IVIF methods. We selected 15 pairs of representative images from 10 datasets and invited 15 independent participants (including 5 domain experts and 10 non-experts) to perform a double-blind evaluation. The evaluators were asked to rank their preferences for each pair of fused images (10 images in total). The final results were obtained by normalizing the preference rankings of all evaluators and calculating the average ranking for each fused image pair.

Fig. 5 shows the preference ranking heatmap for different methods on three datasets. The color intensity in the heatmap visually reflects the performance of each method, with yellow indicating the best and purple indicating the worst. From the heatmap, it is evident that our method achieves higher average rankings across all datasets, demonstrating that the fused images generated by our method better align with human preferences.

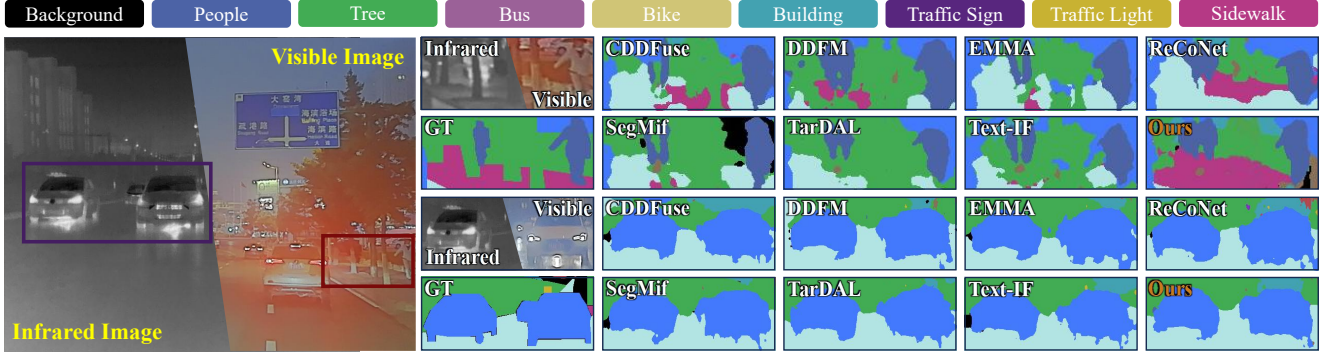


Figure 6. Qualitative comparison of our method with the fusion images generated by different fusion methods on the FMB dataset. Our approach performs the best segmentation results.



Figure 7. Qualitative comparison of our method with the fusion images generated by different fusion methods on the M³FD dataset. Our method achieves the best detection results.

4.4. Downstream IVIF Applications

We further explored the performance of the fused images in downstream tasks, using the FMB and M³FD datasets for semantic segmentation and object detection.

Fig. 6 and Fig. 7 show the qualitative evaluation results for segmentation and detection tasks. For semantic segmentation, our method demonstrates higher classification accuracy in both low-light and high-light scenes. For object detection, our method successfully detects the motorbike in low-light conditions and accurately detects people in the fog under dense fog conditions, while other methods missed some targets. Tab. 3 presents the quantitative results for both tasks. For semantic segmentation, our method outperforms other methods across multiple classification tasks. For key targets such as car and person, our segmentation accuracy ranks first. For object detection, our method achieves the highest mAP. It ranks first in four detection categories, indicating its ability to provide richer feature information and improve detection accuracy.

4.5. Ablation studies

Key Components Ablation. To validate the effectiveness of each component in our proposed framework, we conducted comprehensive ablation studies. First, for the fusion-

oriented reward model, we removed the score prediction branch and the heatmap prediction branch separately. Secondly, during the fine-tuning process, we removed the SAM segmentation and replaced the semantic regions with randomly cropped source image patches. Fig. 8 shows the results of the ablation experiments. Our method preserves clear details under low-light conditions. Removing the score prediction and heatmap prediction branches leads to blurred vehicle edges and artifacts, as the reward model cannot fully evaluate the fused image quality. Removing SAM segmentation lacks weighted optimization for important semantic regions, resulting in worse performance compared to our method. Tab. 4 qualitatively shows the results of the ablation experiments on three datasets. Our method consistently demonstrated the best performance on all three datasets, and the removal of any module led to a decline in the corresponding metrics. This validates the effectiveness of each module in our method.

Policy Optimization Strategy Ablation. We conducted ablation experiments to validate the effectiveness of our proposed fusion method based on GRPO fine-tuning and human feedback guidance. For comparison, we compare the Direct Preference Optimization (DPO) [44] and Proximal Policy Optimization (PPO) [45] optimization base-

Table 3. Quantitative comparison of our method and existing image fusion methods on downstream segmentation and detection tasks on FMB and M³FD. **Red** and **blue** represent the best and second-best results.

Method	FMB							M ³ FD						
	Person	Car	Sky	Bus	Motor	Pole	mIoU	People	Car	Bus	Light	Motor	Trunk	mAP
CDDFuse [68]	63.38	81.59	93.68	56.60	26.05	41.04	55.39	73.06	82.32	67.64	40.03	31.61	55.07	58.29
DDFM [69]	63.26	81.64	94.61	63.34	25.71	42.60	56.64	71.84	83.42	76.42	45.61	34.19	55.47	61.16
EMMA [70]	63.10	80.95	93.85	62.90	26.96	40.92	56.00	72.11	82.32	75.65	36.24	33.33	54.11	58.96
LRRNet [15]	63.58	81.62	94.06	64.28	27.47	40.59	56.37	71.27	83.56	76.41	38.89	<u>36.15</u>	54.25	60.09
MRFS [64]	63.79	81.13	94.01	56.76	27.33	41.35	54.61	68.95	81.53	65.84	35.80	32.35	55.84	56.72
PromptF [28]	63.80	80.66	93.91	55.47	27.88	40.67	55.42	73.50	77.47	76.47	34.82	32.14	48.72	56.69
ReCoNet [11]	62.25	81.17	93.85	63.97	27.73	40.76	56.38	70.64	82.70	69.77	36.77	32.35	53.73	57.66
SegMif [27]	64.21	80.89	94.06	55.39	<u>28.65</u>	42.04	55.99	73.58	84.38	76.47	40.10	35.46	<u>57.02</u>	<u>61.17</u>
SHIP [71]	64.49	80.94	94.04	56.78	25.28	41.55	55.68	73.05	81.50	67.32	42.79	31.37	55.09	58.52
TarDAL [26]	<u>64.80</u>	79.73	94.06	52.99	26.91	39.97	54.15	72.90	81.62	70.26	35.33	22.35	51.17	55.61
Text-IF [61]	64.58	80.77	93.85	60.56	28.53	42.43	56.41	<u>74.36</u>	82.97	<u>76.48</u>	40.93	34.31	56.36	60.90
TIMFusion [31]	62.06	81.25	93.38	55.53	25.46	41.11	55.01	70.49	77.47	76.47	34.82	32.14	48.72	56.69
DCEvo [30]	63.51	80.37	93.65	52.90	28.35	41.92	55.88	73.27	83.20	66.83	36.78	33.08	56.24	58.23
Ours	64.92	82.96	<u>94.51</u>	<u>64.25</u>	29.75	44.69	56.92	74.43	<u>84.17</u>	76.58	<u>44.74</u>	36.27	57.21	62.23



Figure 8. Comparison between w/o score, w/o heatmap, w/o SAM, and our method.

Table 4. Comparison of ablation studies removed key components.

Method	TNO		RoadScene		M ³ FD	
	CC \uparrow	PSNR \uparrow	CC \uparrow	PSNR \uparrow	CC \uparrow	PSNR \uparrow
w/o Score	0.50	64.21	0.51	60.97	0.58	64.81
w/o Heatmap	0.50	65.17	0.54	61.21	0.60	64.93
w/o SAM	0.48	65.03	0.52	60.92	0.57	63.02
Ours	0.51	65.43	0.56	61.84	0.65	65.09

line methods. Qualitative and quantitative analysis was performed on three datasets. As shown in Fig. 9, our method retains the building contour information in the infrared image as well as the texture and color information in the visible image. It balances the infrared and visible information, generating images that are more aligned with human visual preferences. The qualitative evaluation results in Tab. 5 demonstrate the performance on the three datasets. Compared to the baseline methods, although DPO and PPO methods show improvements, our method performs the best, validating its effectiveness.

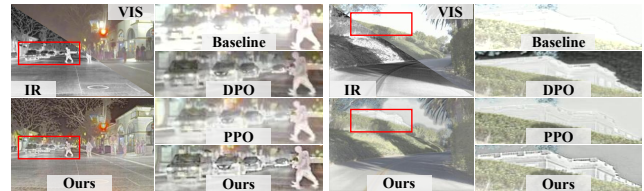


Figure 9. Comparison between the baseline, DPO [44], PPO [45], and our method.

Table 5. Comparison of ablation studies with different fine-tuning methods.

Method	TNO		RoadScene		M ³ FD	
	CC \uparrow	PSNR \uparrow	CC \uparrow	PSNR \uparrow	CC \uparrow	PSNR \uparrow
Baseline	0.48	63.83	0.49	59.66	0.55	62.87
DPO	0.50	63.98	0.49	61.50	0.57	63.74
PPO	0.51	63.59	0.53	61.17	0.59	64.32
Ours	0.51	65.43	0.56	61.84	0.65	65.09

5. Conclusion

We propose a fusion method based on RLHF that aligns image fusion quality with human visual preferences through human feedback. On the one hand, we design a human feedback dataset that includes multidimensional scores and image artifact annotations, and train a Fusion-Oriented reward model, filling the gap in existing IVIF research regarding datasets and metrics related to human preferences. On the other hand, by combining the trained reward model and inspired by GRPO, we fine-tune the IVIF task, overcoming the limitations of traditional fusion networks in capturing human visual preferences. In the end, the generated fused images are more aligned with human visual preferences, significantly improving the quality of the fused images.

References

- [1] Jinze Bai, Shuai Bai, Yunfei Chu, Zeyu Cui, Kai Dang, Xiaodong Deng, Yang Fan, Wenbin Ge, Yu Han, Fei Huang, et al. Qwen technical report. *arXiv preprint arXiv:2309.16609*, 2023. 2
- [2] Bing Cao, Xingxin Xu, Pengfei Zhu, Qilong Wang, and Qinghua Hu. Conditional controllable image fusion. *arXiv preprint arXiv:2411.01573*, 2024. 2
- [3] Le Chang, Yongdong Huang, Qiufu Li, Weijian Su, and Yuduo Zhang. L 2 net: Infrared and visible image fusion using lightweight large kernel convolution network. *IEEE Transactions on Instrumentation and Measurement*, 72:1–13, 2023. 2
- [4] Zizhao Chen, Yeqiang Qian, Xiaoxiao Yang, Chunxiang Wang, and Ming Yang. Amfd: Distillation via adaptive multimodal fusion for multispectral pedestrian detection. *arXiv preprint arXiv:2405.12944*, 2024. 3
- [5] Chunyang Cheng, Tianyang Xu, Xiao-Jun Wu, Hui Li, Xi Li, and Josef Kittler. Fusionbooster: A unified image fusion boosting paradigm. *International Journal of Computer Vision*, 133(5):3041–3058, 2025. 2
- [6] Paul F Christiano, Jan Leike, Tom Brown, Miljan Martic, Shane Legg, and Dario Amodei. Deep reinforcement learning from human preferences. *Advances in neural information processing systems*, 30, 2017. 2
- [7] Zhenbang Du, Wei Feng, Haohan Wang, Yaoyu Li, Jingsen Wang, Jian Li, Zheng Zhang, Jingjing Lv, Xin Zhu, Junsheng Jin, et al. Towards reliable advertising image generation using human feedback. In *European Conference on Computer Vision*, pages 399–415. Springer, 2024. 3
- [8] Ying Fan, Olivia Watkins, Yuqing Du, Hao Liu, Moonkyung Ryu, Craig Boutilier, Pieter Abbeel, Mohammad Ghavamzadeh, Kangwook Lee, and Kimin Lee. Dpok: Reinforcement learning for fine-tuning text-to-image diffusion models. *Advances in Neural Information Processing Systems*, 36:79858–79885, 2023. 3
- [9] Chengyu Fang, Chunming He, Longxiang Tang, Yuelin Zhang, Chenyang Zhu, Yuqi Shen, Chubin Chen, Guoxia Xu, and Xiu Li. Integrating extra modality helps segmentor find camouflaged objects well. *arXiv preprint arXiv:2502.14471*, 2025. 1
- [10] Qishen Ha, Kohei Watanabe, Takumi Karasawa, Yoshitaka Ushiku, and Tatsuya Harada. Mfnet: Towards real-time semantic segmentation for autonomous vehicles with multispectral scenes. In *2017 IEEE/RSJ International Conference on Intelligent Robots and Systems (IROS)*, pages 5108–5115. IEEE, 2017. 3
- [11] Zhanbo Huang, Jinyuan Liu, Xin Fan, Risheng Liu, Wei Zhong, and Zhongxuan Luo. Reconet: Recurrent correction network for fast and efficient multi-modality image fusion. In *European conference on computer vision*, pages 539–555. Springer, 2022. 5, 6, 8
- [12] Aaron Hurst, Adam Lerer, Adam P Goucher, Adam Perelman, Aditya Ramesh, Aidan Clark, AJ Ostrow, Akila Welihinda, Alan Hayes, Alec Radford, et al. Gpt-4o system card. *arXiv preprint arXiv:2410.21276*, 2024. 3
- [13] Xinyu Jia, Chuang Zhu, Minzhen Li, Wenqi Tang, and Wenli Zhou. Llvip: A visible-infrared paired dataset for low-light vision. In *Proceedings of the IEEE/CVF international conference on computer vision*, pages 3496–3504, 2021. 3
- [14] Alexander Kirillov, Eric Mintun, Nikhila Ravi, Hanzi Mao, Chloe Rolland, Laura Gustafson, Tete Xiao, Spencer Whitehead, Alexander C Berg, Wan-Yen Lo, et al. Segment anything. In *Proceedings of the IEEE/CVF international conference on computer vision*, pages 4015–4026, 2023. 4
- [15] Hui Li, Tianyang Xu, Xiao-Jun Wu, Jiwen Lu, and Josef Kittler. Lrrnet: A novel representation learning guided fusion network for infrared and visible images. *IEEE transactions on pattern analysis and machine intelligence*, 45(9):11040–11052, 2023. 1, 5, 6, 8
- [16] Huafeng Li, Junyu Liu, Yafei Zhang, and Yu Liu. A deep learning framework for infrared and visible image fusion without strict registration. *International Journal of Computer Vision*, 132(5):1625–1644, 2024. 2
- [17] Huafeng Li, Zengyi Yang, Yafei Zhang, Wei Jia, Zhengtao Yu, and Yu Liu. Mulfs-cap: Multimodal fusion-supervised cross-modality alignment perception for unregistered infrared-visible image fusion. *IEEE Transactions on Pattern Analysis and Machine Intelligence*, 2025. 2
- [18] Jing Li, Hongtao Huo, Chang Li, Renhua Wang, and Qi Feng. Attentionfgan: Infrared and visible image fusion using attention-based generative adversarial networks. *IEEE Transactions on Multimedia*, 23:1383–1396, 2020. 2
- [19] Jiawei Li, Jiansheng Chen, Jinyuan Liu, and Huimin Ma. Learning a graph neural network with cross modality interaction for image fusion. In *Proceedings of the 31st ACM international conference on multimedia*, pages 4471–4479, 2023. 2
- [20] Jiayang Li, Junjun Jiang, Pengwei Liang, Jiayi Ma, and Liqiang Nie. Maefuse: Transferring omni features with pre-trained masked autoencoders for infrared and visible image fusion via guided training. *IEEE Transactions on Image Processing*, 2025. 2
- [21] Xingyuan Li, Yang Zou, Jinyuan Liu, Zhiying Jiang, Long Ma, Xin Fan, and Risheng Liu. From text to pixels: A context-aware semantic synergy solution for infrared and visible image fusion. *arXiv preprint arXiv:2401.00421*, 2023. 2
- [22] Xingyuan Li, Jinyuan Liu, Zhixin Chen, Yang Zou, Long Ma, Xin Fan, and Risheng Liu. Contourlet residual for prompt learning enhanced infrared image super-resolution. In *European Conference on Computer Vision*, pages 270–288. Springer, 2024. 1
- [23] Xingyuan Li, Zirui Wang, Yang Zou, Zhixin Chen, Jun Ma, Zhiying Jiang, Long Ma, and Jinyuan Liu. Difisir: A diffusion model with gradient guidance for infrared image super-resolution. In *Proceedings of the Computer Vision and Pattern Recognition Conference*, pages 7534–7544, 2025. 1
- [24] Youwei Liang, Junfeng He, Gang Li, Peizhao Li, Arseniy Klimovskiy, Nicholas Carolan, Jiao Sun, Jordi Pont-Tuset, Sarah Young, Feng Yang, et al. Rich human feedback for text-to-image generation. In *Proceedings of the IEEE/CVF Conference on Computer Vision and Pattern Recognition*, pages 19401–19411, 2024. 3

- [25] Aixin Liu, Bei Feng, Bing Xue, Bingxuan Wang, Bochao Wu, Chengda Lu, Chenggang Zhao, Chengqi Deng, Chenyu Zhang, Chong Ruan, et al. Deepseek-v3 technical report. *arXiv preprint arXiv:2412.19437*, 2024. 2
- [26] Jinyuan Liu, Xin Fan, Zhanbo Huang, Guanyao Wu, Risheng Liu, Wei Zhong, and Zhongxuan Luo. Target-aware dual adversarial learning and a multi-scenario multi-modality benchmark to fuse infrared and visible for object detection. In *Proceedings of the IEEE/CVF conference on computer vision and pattern recognition*, pages 5802–5811, 2022. 1, 3, 5, 6, 8
- [27] Jinyuan Liu, Zhu Liu, Guanyao Wu, Long Ma, Risheng Liu, Wei Zhong, Zhongxuan Luo, and Xin Fan. Multi-interactive feature learning and a full-time multi-modality benchmark for image fusion and segmentation. In *Proceedings of the IEEE/CVF international conference on computer vision*, pages 8115–8124, 2023. 1, 3, 5, 6, 8
- [28] Jinyuan Liu, Xingyuan Li, Zirui Wang, Zhiying Jiang, Wei Zhong, Wei Fan, and Bin Xu. Promptfusion: Harmonized semantic prompt learning for infrared and visible image fusion. *IEEE/CAA Journal of Automatica Sinica*, 2024. 1, 2, 3, 5, 6, 8
- [29] Jinyuan Liu, Runjia Lin, Guanyao Wu, Risheng Liu, Zhongxuan Luo, and Xin Fan. Coconet: Coupled contrastive learning network with multi-level feature ensemble for multi-modality image fusion. *International Journal of Computer Vision*, 132(5):1748–1775, 2024. 2, 3
- [30] Jinyuan Liu, Bowei Zhang, Qingyun Mei, Xingyuan Li, Yang Zou, Zhiying Jiang, Long Ma, Risheng Liu, and Xin Fan. Dcevo: Discriminative cross-dimensional evolutionary learning for infrared and visible image fusion. *arXiv preprint arXiv:2503.17673*, 2025. 4, 5, 6, 8
- [31] Risheng Liu, Zhu Liu, Jinyuan Liu, Xin Fan, and Zhongxuan Luo. A task-guided, implicitly-searched and metainitialized deep model for image fusion. *IEEE Transactions on Pattern Analysis and Machine Intelligence*, 2024. 2, 5, 6, 8
- [32] Jiayi Ma, Wei Yu, Pengwei Liang, Chang Li, and Junjun Jiang. Fusiongan: A generative adversarial network for infrared and visible image fusion. *Information fusion*, 48:11–26, 2019. 1, 2
- [33] Jiayi Ma, Hao Zhang, Zhenfeng Shao, Pengwei Liang, and Han Xu. Ganmcc: A generative adversarial network with multiclassification constraints for infrared and visible image fusion. *IEEE Transactions on Instrumentation and Measurement*, 70:1–14, 2020. 2
- [34] Jiayi Ma, Linfeng Tang, Meilong Xu, Hao Zhang, and Guobao Xiao. Stdffusionnet: An infrared and visible image fusion network based on salient target detection. *IEEE Transactions on Instrumentation and Measurement*, 70:1–13, 2021. 2
- [35] Jiayi Ma, Linfeng Tang, Fan Fan, Jun Huang, Xiaoguang Mei, and Yong Ma. Swinfusion: Cross-domain long-range learning for general image fusion via swin transformer. *IEEE/CAA Journal of Automatica Sinica*, 9(7):1200–1217, 2022. 2
- [36] Yue Ma, Yingqing He, Xiaodong Cun, Xintao Wang, Siran Chen, Xiu Li, and Qifeng Chen. Follow your pose: Pose-guided text-to-video generation using pose-free videos. In *Proceedings of the AAAI Conference on Artificial Intelligence*, pages 4117–4125, 2024. 1
- [37] Anish Mittal, Anush Krishna Moorthy, and Alan Conrad Bovik. No-reference image quality assessment in the spatial domain. *IEEE Transactions on image processing*, 21(12):4695–4708, 2012. 6
- [38] Anish Mittal, Rajiv Soundararajan, and Alan C Bovik. Making a “completely blind” image quality analyzer. *IEEE Signal processing letters*, 20(3):209–212, 2012. 6
- [39] Long Ouyang, Jeffrey Wu, Xu Jiang, Diogo Almeida, Carroll Wainwright, Pamela Mishkin, Chong Zhang, Sandhini Agarwal, Katarina Slama, Alex Ray, et al. Training language models to follow instructions with human feedback. *Advances in neural information processing systems*, 35:27730–27744, 2022. 2
- [40] Seonghyun Park, An Gia Vien, and Chul Lee. Cross-modal transformers for infrared and visible image fusion. *IEEE Transactions on Circuits and Systems for Video Technology*, 34(2):770–785, 2023. 2
- [41] Xinran Qin, Yuhui Quan, Zhuojie Chen, and Hui Ji. Robust unsupervised deep learning for nonblind image deconvolution with inaccurate kernels. *IEEE Transactions on Neural Networks and Learning Systems*, 2025. 1
- [42] Xinran Qin, Yuning Cui, Shangquan Sun, Ruoyu Chen, Wenqi Ren, Alois Knoll, and Xiaochun Cao. Disentangle to fuse: Towards content preservation and cross-modality consistency for multi-modality image fusion. *IEEE Transactions on Image Processing*, 2026. 1
- [43] Yuhui Quan, Xinran Qin, Tongyao Pang, and Hui Ji. Siamese cooperative learning for unsupervised image reconstruction from incomplete measurements. *IEEE Transactions on Pattern Analysis and Machine Intelligence*, 46(7):4866–4879, 2024. 1
- [44] Rafael Rafailov, Archit Sharma, Eric Mitchell, Christopher D Manning, Stefano Ermon, and Chelsea Finn. Direct preference optimization: Your language model is secretly a reward model. *Advances in Neural Information Processing Systems*, 36:53728–53741, 2023. 7, 8
- [45] John Schulman, Filip Wolski, Prafulla Dhariwal, Alec Radford, and Oleg Klimov. Proximal policy optimization algorithms. *arXiv preprint arXiv:1707.06347*, 2017. 7, 8
- [46] Zhihong Shao, Peiyi Wang, Qihao Zhu, Runxin Xu, Junxiao Song, Xiao Bi, Haowei Zhang, Mingchuan Zhang, YK Li, Y Wu, et al. Deepseekmath: Pushing the limits of mathematical reasoning in open language models. *arXiv preprint arXiv:2402.03300*, 2024. 4
- [47] Yu Shi, Yu Liu, Juan Cheng, Z Jane Wang, and Xun Chen. Vdmufusion: A versatile diffusion model-based unsupervised framework for image fusion. *IEEE Transactions on Image Processing*, 34:441–454, 2024. 2
- [48] Yiming Sun, Bing Cao, Pengfei Zhu, and Qinghua Hu. Defusion: A detection-driven infrared and visible image fusion network. In *Proceedings of the 30th ACM international conference on multimedia*, pages 4003–4011, 2022. 2
- [49] Linfeng Tang, Jiteng Yuan, Hao Zhang, Xingyu Jiang, and Jiayi Ma. Piafusion: A progressive infrared and visible image fusion network based on illumination aware. *Information Fusion*, 83:79–92, 2022. 5

- [50] Linfeng Tang, Hao Zhang, Han Xu, and Jiayi Ma. Rethinking the necessity of image fusion in high-level vision tasks: A practical infrared and visible image fusion network based on progressive semantic injection and scene fidelity. *Information Fusion*, 99:101870, 2023. 2
- [51] Alexander Toet. The tno multiband image data collection. *Data in brief*, 15:249, 2017. 3, 5
- [52] Hugo Touvron, Louis Martin, Kevin Stone, Peter Albert, Amjad Almahairi, Yasmine Babaei, Nikolay Bashlykov, Soumya Batra, Prajjwal Bhargava, Shruti Bhosale, et al. Llama 2: Open foundation and fine-tuned chat models. *arXiv preprint arXiv:2307.09288*, 2023. 2
- [53] Zhou Wang, Alan C Bovik, Hamid R Sheikh, and Eero P Simoncelli. Image quality assessment: from error visibility to structural similarity. *IEEE transactions on image processing*, 13(4):600–612, 2004. 6
- [54] Zirui Wang, Jiayi Zhang, Tianwei Guan, Yuhan Zhou, Xingyuan Li, Minjing Dong, and Jinyuan Liu. Efficient rectified flow for image fusion. *arXiv preprint arXiv:2509.16549*, 2025. 2
- [55] Dan Wu, Mina Han, Yang Yang, Shan Zhao, Yujing Rao, Hao Li, Xing Lin, Chengjiang Zhou, and Haicheng Bai. Dc-fusion: A dual-frequency cross-enhanced fusion network for infrared and visible image fusion. *IEEE Transactions on Instrumentation and Measurement*, 72:1–15, 2023. 2
- [56] Han Xu, Pengwei Liang, Wei Yu, Junjun Jiang, and Jiayi Ma. Learning a generative model for fusing infrared and visible images via conditional generative adversarial network with dual discriminators. In *IJCAI*, pages 3954–3960, 2019. 1, 3
- [57] Han Xu, Jiayi Ma, Junjun Jiang, Xiaojie Guo, and Haibin Ling. U2fusion: A unified unsupervised image fusion network. *IEEE Transactions on Pattern Analysis and Machine Intelligence*, 2020. 1, 3, 5
- [58] Han Xu, Jiteng Yuan, and Jiayi Ma. Murf: Mutually reinforcing multi-modal image registration and fusion. *IEEE transactions on pattern analysis and machine intelligence*, 45(10):12148–12166, 2023. 3
- [59] Jiazheng Xu, Xiao Liu, Yuchen Wu, Yuxuan Tong, Qinkai Li, Ming Ding, Jie Tang, and Yuxiao Dong. Imagereward: Learning and evaluating human preferences for text-to-image generation. *Advances in Neural Information Processing Systems*, 36:15903–15935, 2023. 3
- [60] Zengyi Yang, Yafei Zhang, Huafeng Li, and Yu Liu. Instruction-driven fusion of infrared-visible images: Tailoring for diverse downstream tasks. *Information Fusion*, 121:103148, 2025. 1
- [61] Xunpeng Yi, Han Xu, Hao Zhang, Linfeng Tang, and Jiayi Ma. Text-if: Leveraging semantic text guidance for degradation-aware and interactive image fusion. In *Proceedings of the IEEE/CVF Conference on Computer Vision and Pattern Recognition*, pages 27026–27035, 2024. 1, 3, 5, 6, 8
- [62] Zhenjie Yu, Shuang Li, Yirui Shen, Chi Harold Liu, and Shuigen Wang. On the difficulty of unpaired infrared-to-visible video translation: fine-grained content-rich patches transfer. In *Proceedings of the IEEE/CVF Conference on Computer Vision and Pattern Recognition*, pages 1631–1640, 2023. 1
- [63] Hangjie Yuan, Shiwei Zhang, Xiang Wang, Yujie Wei, Tao Feng, Yining Pan, Yingya Zhang, Ziwei Liu, Samuel Albanie, and Dong Ni. Instructvideo: Instructing video diffusion models with human feedback. In *Proceedings of the IEEE/CVF Conference on Computer Vision and Pattern Recognition (CVPR)*, pages 6463–6474, 2024. 3
- [64] Hao Zhang, Xuhui Zuo, Jie Jiang, Chunchao Guo, and Jiayi Ma. Mrfs: Mutually reinforcing image fusion and segmentation. In *Proceedings of the IEEE/CVF Conference on Computer Vision and Pattern Recognition*, pages 26974–26983, 2024. 5, 6, 8
- [65] Xingchen Zhang, Ping Ye, and Gang Xiao. Vifb: A visible and infrared image fusion benchmark. In *Proceedings of the IEEE/CVF Conference on Computer Vision and Pattern Recognition Workshops*, 2020. 3
- [66] Zeyang Zhang, Hui Li, Tianyang Xu, Xiao-Jun Wu, and Josef Kittler. Ddbfusion: An unified image decomposition and fusion framework based on dual decomposition and bézier curves. *Information Fusion*, 114:102655, 2025. 1
- [67] Wenda Zhao, Shigeng Xie, Fan Zhao, You He, and Huchuan Lu. Metafusion: Infrared and visible image fusion via meta-feature embedding from object detection. In *Proceedings of the IEEE/CVF Conference on Computer Vision and Pattern Recognition*, pages 13955–13965, 2023. 3
- [68] Zixiang Zhao, Haowen Bai, Jianshe Zhang, Yulun Zhang, Shuang Xu, Zudi Lin, Radu Timofte, and Luc Van Gool. Cddfuse: Correlation-driven dual-branch feature decomposition for multi-modality image fusion. In *Proceedings of the IEEE/CVF conference on computer vision and pattern recognition*, pages 5906–5916, 2023. 1, 3, 5, 6, 8
- [69] Zixiang Zhao, Haowen Bai, Yuanzhi Zhu, Jianshe Zhang, Shuang Xu, Yulun Zhang, Kai Zhang, Deyu Meng, Radu Timofte, and Luc Van Gool. Ddfm: denoising diffusion model for multi-modality image fusion. In *Proceedings of the IEEE/CVF International Conference on Computer Vision*, pages 8082–8093, 2023. 2, 3, 5, 6, 8
- [70] Zixiang Zhao, Haowen Bai, Jianshe Zhang, Yulun Zhang, Kai Zhang, Shuang Xu, Dongdong Chen, Radu Timofte, and Luc Van Gool. Equivariant multi-modality image fusion. In *Proceedings of the IEEE/CVF conference on computer vision and pattern recognition*, pages 25912–25921, 2024. 5, 6, 8
- [71] Naishan Zheng, Man Zhou, Jie Huang, Junming Hou, Haoying Li, Yuan Xu, and Feng Zhao. Probing synergistic high-order interaction in infrared and visible image fusion. In *Proceedings of the IEEE/CVF conference on computer vision and pattern recognition*, pages 26384–26395, 2024. 5, 6, 8
- [72] Yang Zou, Zhixin Chen, Zhipeng Zhang, Xingyuan Li, Long Ma, Jinyuan Liu, Peng Wang, and Yanning Zhang. Contourlet refinement gate framework for thermal spectrum distribution regularized infrared image super-resolution. *International Journal of Computer Vision*, 134(1):23, 2026. 1